Model-based redatuming of seismic data: an inverse filter approach

Thomas Planès[1,2], Roel Snieder[1] and Satyan Singh[1,3]

(1) Center for Wave Phenomena and Dept. of Geophysics, Colorado School of Mines, Golden CO 80401
email rsnieder@mines.edu
(2) Now at the University of Geneva, tho.planes@gmail.com
(3) Now at the University of Edinburgh, satyansinghster@gmail.com

ABSTRACT
Standard model-based redatuming techniques consist in applying time shifts to the surface data, to simulate an acquisition made at depth. The time shifts are computed using prior knowledge of the overburden, such as a macro velocity model. These techniques allow focusing of the direct waves at the new datum, but the focus can be degraded because of surface multiples and internal multiples in the overburden. We show that if the medium above the redatuming level is known, these multiples can be removed. We compute exact focusing functions, free of multiples, using an inverse-filter approach. These focusing functions create downgoing and upgoing virtual sources at the new datum. The surface responses to these virtual sources are then used to compute the objective redatumed data set through multi-dimensional deconvolution. The redatumed data set corresponds to a virtual acquisition made at the new datum and for which the imprint of the overburden is completely removed. We demonstrate the technique on 2D acoustic synthetic examples corresponding to a seismic context and an acoustic nondestructive testing context.

Key words: downward continuation, redatuming

1 INTRODUCTION

Redatuming seismic data consists in virtually moving the sources and receivers from the original acquisition level to a new depth level, also called new datum. This process can be employed when the original acquisition grid is inadequate for imaging purposes, as in cases of rugged topography, irregular spatial sampling, remoteness from target, etc.

When buried sensors are available at the new datum (e.g., in a deviated well), creating virtual sources can be achieved based on the data only, without any prior knowledge of the medium. Processing techniques have been developed for this purpose and fall into the category of correlation-based redatuming Schuster and Zhou (2006).

When buried sensors are not available, model-based redatuming relies on applying corrections to the original data set based on some prior knowledge of the overburden - i.e., some knowledge of the medium parameters between the original and the new datum. The standard approach consists in modeling the propagation of the direct waves between the surface and the positions of the virtual sources/receivers, and in applying corresponding time shifts to the data Berryhill (1979); Shtivelman and Canning (1988). This approach only requires a macro velocity model of the overburden as prior information.

The standard model-based redatuming methods can successfully focus the direct waves at the new datum but do not account for surface multiples and internal multiples in the overburden. These multiples can generate ghost arrivals in the redatumed data set and thus ghost reflectors in the subsequent images.

In the field of acoustics, a similar problematic of imperfect focusing led to the development of the spatio-temporal inverse-filter technique Tanter et al. (2001). With a single-sided source distribution, this technique aims to focus acoustic wavefields beyond complicated layers for medical imaging and nondestructive testing purposes Aubry et al. (2001). It requires the acquisition of a baseline data set, for which the "overburden" is extracted from the rest of the medium. With sources on one side and receivers on the other side of the over-

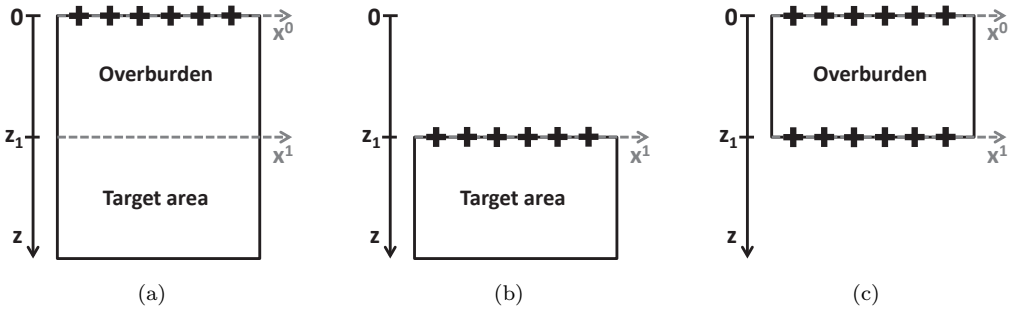

Figure 1. (a) Full medium with free surface, overburden, and target area. (b) Objective medium with target area below the new datum $z = z_1$ and homogeneous above. (c) Priorly known upper medium with free surface, overburden, and homogeneous below the new datum $z = z_1$. The (virtual) sources and receivers are denoted by the black crosses.

burden, a transmission matrix is acquired and focusing functions are built through an inversion procedure.

In a seismic context, a physical acquisition of such a baseline is not possible. However, if one has a good knowledge of the medium parameters in the overburden, the transmission matrix can be computed numerically. This is the approach that we use here to compute focusing functions that give rise to upgoing and downgoing virtual sources at the new datum.

Note that the Marchenko imaging procedure aims to iteratively infer these same focusing functions, only using a macro velocity model and reflected waves recorded at the surface as prior information Wapenaar et al. (2013); Broggini et al. (2014). The method we propose here thus requires more prior information than the Marchenko method but can provide in turn a simpler, more direct way to compute these focusing functions.

Once the responses to the upgoing and downgoing virtual sources are known, the imprint of the overburden can be fully removed through multi-dimensional deconvolution Schuster and Zhou (2006); Wapenaar et al. (2008); Wapenaar and van der Neut (2010). Our work is related to the "rigorous redatuming" method developed by Mulder (2005), that requires similar assumptions and aims at the same objective. However, we follow a different approach and our formalism involves one less inversion step in the redatuming procedure.

The formal derivation of the redatuming equations, based on Rayleigh's reciprocity theorem, is presented in the appendix. In the main text, we provide a heuristic graphics-based derivation that relies on a matrix formalism. We then demonstrate the method on two synthetic data sets: one corresponding to a seismic context; and the other one corresponding to an acoustic nondestructive testing context. In both cases, we successfully retrieve redatumed Green's functions for which the imprint of the overburden is removed.

2 THEORY

We consider a 2D acoustic medium with variable density $\rho(\boldsymbol{r})$ and compression modulus $\kappa(\boldsymbol{r})$. The frequency-domain wave equation for the pressure $p(\boldsymbol{r},\omega)$ reads

$$\rho(\boldsymbol{r})\boldsymbol{\nabla}.\left[\frac{1}{\rho(\boldsymbol{r})}\boldsymbol{\nabla}p(\boldsymbol{r},\omega)\right]+\frac{\omega^2}{c^2(\boldsymbol{r})}p(\boldsymbol{r},\omega)=f(\boldsymbol{r},\omega)\ , \quad (1)$$

where ω is the angular frequency, $c(\boldsymbol{r})=\sqrt{\kappa/\rho}$ is the medium velocity and $f(\boldsymbol{r},\omega)$ an arbitrary source term. We define the Green's function $g(\boldsymbol{r},\boldsymbol{r_s},\omega)$ as the solution of this wave equation for a monopole Dirac source term at $\boldsymbol{r_s}$, i.e.,

$$\boldsymbol{\nabla}.\left[\frac{1}{\rho(\boldsymbol{r})}\boldsymbol{\nabla}g(\boldsymbol{r},\boldsymbol{r_s})\right]+\frac{\omega^2}{\kappa(\boldsymbol{r})}g(\boldsymbol{r},\boldsymbol{r_s})=\delta(\boldsymbol{r}-\boldsymbol{r_s})\ , \quad (2)$$

where the frequency dependency of the Green's functions is made implicit from now on. Note that the density has been included in the source term, so that the Green's function is the solution of the wave equation (equation 1) with a source term $f(\boldsymbol{r},\omega)=\rho(\boldsymbol{r})\delta(\boldsymbol{r}-\boldsymbol{r_s})$. In the absence of horizontally propagating waves, the Green's function can be decomposed at the receiver level into an upgoing part and a downgoing part as

$$g(\boldsymbol{r},\boldsymbol{r_s})=g^{+,p}(\boldsymbol{r},\boldsymbol{r_s})+g^{-,p}(\boldsymbol{r},\boldsymbol{r_s})\ , \quad (3)$$

where $g^{+,p}(\boldsymbol{r},\boldsymbol{r_s})$ represents the downgoing pressure wavefield at $\boldsymbol{r}$ (superscript $+$) for an impulse pressure source at $\boldsymbol{r_s}$ (superscript p) and where $g^{-,p}(\boldsymbol{r},\boldsymbol{r_s})$ represents the upgoing pressure wavefield at $\boldsymbol{r}$ (superscript $-$) for an impulse pressure source at $\boldsymbol{r_s}$ (superscript p). The Green's functions can also be decomposed at the source level as

$$g(\boldsymbol{r},\boldsymbol{r_s})=g^{p,+}(\boldsymbol{r},\boldsymbol{r_s})+g^{p,-}(\boldsymbol{r},\boldsymbol{r_s})\ , \quad (4)$$

where $g^{p,+}(\boldsymbol{r},\boldsymbol{r_s})$ represents the full pressure wavefield at $\boldsymbol{r}$ (superscript p) for a downgoing pressure source at $\boldsymbol{r_s}$ (superscript $+$) and where $g^{p,-}(\boldsymbol{r},\boldsymbol{r_s})$ represents the full pressure wavefield at $\boldsymbol{r}$ (superscript p) for an upgoing pressure source at $\boldsymbol{r_s}$ (superscript $-$). By reciprocity,

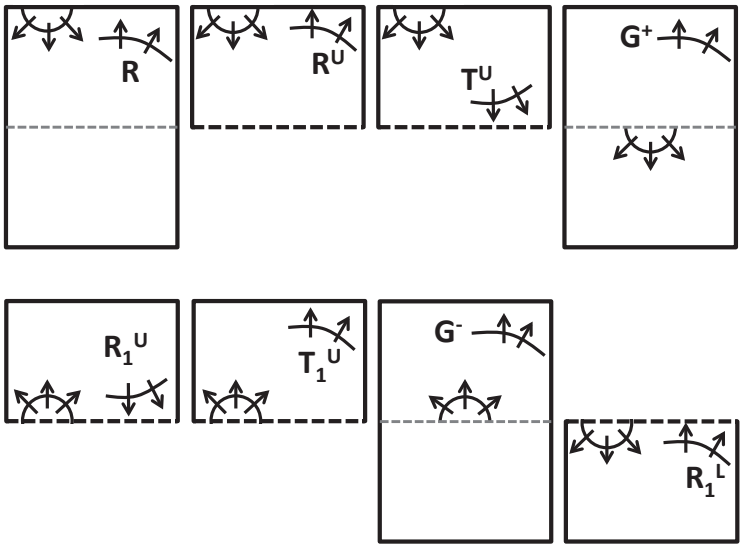

Figure 2. Graphical representation of the Green's function matrices used in the redatuming procedure.

we have

$$\begin{aligned} g(\boldsymbol{r},\boldsymbol{r_s}) &= g(\boldsymbol{r_s},\boldsymbol{r}) \ , \\ g^{+,p}(\boldsymbol{r},\boldsymbol{r_s}) &= g^{p,-}(\boldsymbol{r_s},\boldsymbol{r}) \ , \\ g^{-,p}(\boldsymbol{r},\boldsymbol{r_s}) &= g^{p,+}(\boldsymbol{r_s},\boldsymbol{r}) \ . \end{aligned} \tag{5}$$

We consider N sources and N receivers at coincident locations just below the free surface, and whose positions are described by the coordinate x^0 (Figure 1(a)). We define the $N \times N$ reflection matrix $\mathbf{R}$ of the full medium as $R_{ij} = g(x_i^0, x_j^0, \omega)$. It contains the responses from each source position x_j^0 to each receiver position x_i^0 and corresponds to a reflection data set acquired at the free surface.

Our objective is to transform the initial reflection data set $\mathbf{R}$ into a virtual reflection data set $\mathbf{R_1^L}$, corresponding to virtual sources and receivers located at depth z_1 and for which the imprint of the overburden (medium above z_1) is completely removed. This amounts to retrieving the $N \times N$ reflection matrix $\mathbf{R_1^L}$ of the objective medium represented in Figure 1(b), that is homogeneous above the new datum z_1. The superscript L denotes quantities corresponding to this objective (or lower) medium, and we define $\{\mathbf{R_1^L}\}_{ij} = -(4(\Delta x)^2/\rho(x_i^1)\rho(x_j^1))\partial_z g^{\mathrm{L}}(x_i^1, x_j^1, \omega)$. The positions of the N virtual sources and receivers at depth z_1 (the new datum) are described by the coordinate x^1, and Δx is the spatial pitch of these virtual sensors.

The formal derivation of the redatuming procedure is based on Rayleigh's reciprocity theorem and is presented in Appendices A and B. The formulation of the redatuming equations into simple matrix relations explains the peculiar definition of matrix $\mathbf{R_1^L}$. In the following, we propose a heuristic, graphics-based illustration of these redatuming equations. The matrices $\mathbf{R}$ and $\mathbf{R_1^L}$ are schematized in Figure 2.

We define $\mathbf{G}^+$ (resp. $\mathbf{G}^-$) as Green's function matrices in the full medium (Figure 1(a)) for downgoing (resp. upgoing) sources located at depth z_1, so that $\{\mathbf{G}^+\}_{ij} = (2\Delta x/\rho(x_j^1))g^{p,+}(x_i^0, x_j^1, \omega)$ and $\{\mathbf{G}^-\}_{ij} = g^{p,-}(x_i^0, x_j^1, \omega)$. These matrices are also schematized in Figure 2. If $\mathbf{G}^+$ and $\mathbf{G}^-$ are known, then the reflection matrix $\mathbf{R_1^L}$ can be obtained from the relation

$$\mathbf{G}^+ = \mathbf{G}^- \mathbf{R_1^L} \quad . \tag{6}$$

This relation is graphically illustrated in Figure 3(a). Because the objective medium is homogeneous above depth z_1 (Figure 1(b)), $\mathbf{R_1^L}$ represents the upgoing wavefield response at z_1 to a downgoing source wavefield at z_1. If these upgoing wavefields are convolved with the upgoing source Green's function matrix $\mathbf{G}^-$, the resulting wavefield recorded at the free surface is equivalent to the downgoing source Green's function matrix $\mathbf{G}^+$.

Note that by virtue of source-receiver reciprocity, knowing $\mathbf{G}^+$ and $\mathbf{G}^-$ is equivalent to measuring upgoing and downgoing wavefields at the new datum, as in a deviated well configuration. Solving for $\mathbf{R_1^L}$ in equation 6 then amounts to a discretized form of multi-dimensional deconvolution Schuster and Zhou (2006); Wapenaar and van der Neut (2010).

Because we do not suppose the physical presence of receivers at depth, we numerically compute $\mathbf{G}^+$ and $\mathbf{G}^-$ using the surface-acquired data set $\mathbf{R}$ and our prior knowledge of the overburden (between $z = 0$ and $z = z_1$). First, we perform numerical simulations in the upper medium depicted in Figure 1(c), that has a free surface at $z = 0$ and that is homogeneous below $z = z_1$. This gives the $N \times N$ reflection and transmission matrices $\mathbf{R^U}$, $\mathbf{R_1^U}$, $\mathbf{T^U}$ and $\mathbf{T_1^U}$, where the superscript U

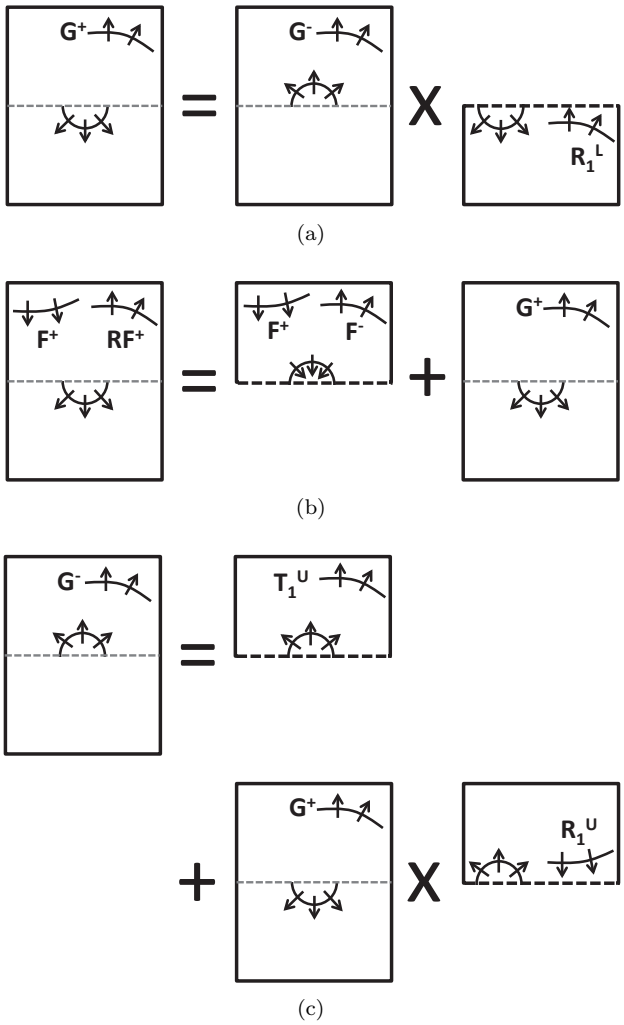

Figure 3. Graphical representation of (a) equation 6, (b) equation 9, and (c) equation 11. To follow the graphics from source to receiver, the matrix products are to be read from right to left .

indicates quantities calculated in this upper medium. These matrices are defined as $\{\mathbf{R^U}\}_{ij} = g^{\mathrm{U}}(x_i^0, x_j^0, \omega)$, $\{\mathbf{R_1^U}\}_{ij} = \partial_z g^{\mathrm{U}}(x_i^1, x_j^1, \omega)$, $\{\mathbf{T^U}\}_{ij} = \partial_z g^{\mathrm{U}}(x_i^1, x_j^0, \omega)$, $\{\mathbf{T_1^U}\}_{ij} = g^{\mathrm{U}}(x_i^0, x_j^1, \omega)$. They are graphically represented in Figure 2.

To compute $\mathbf{G}^+$, we then have to build focusing source functions that, when sent from the free surface, collapse into downgoing Dirac impulses at the new datum. Assuming that these focusing functions exist, they can be gathered in the matrix $\mathbf{F}^+$ so that

$$\mathbf{T^U F}^+ = \mathbf{I} \quad , \tag{7}$$

and because the focusing functions are reflected in the upper medium,

$$\mathbf{R^U F}^+ = \mathbf{F}^- \quad . \tag{8}$$

The identity matrix $\mathbf{I}$ defines a set of objective Dirac impulses at each position on the new datum. Causality and medium homogeneity below z_1 insures that these are downgoing impulses. By definition, $\mathbf{F}^-$ represents the surface response of the focusing functions in the upper medium. The idea of computing the focusing functions $\mathbf{F}^+$ by finding the inverse of the transmission matrix $\mathbf{T^U}$ is at the center of the spatio-temporal inverse-filter technique developed in acoustics Tanter et al. (2001); Aubry et al. (2001). When the transmission matrix of the overburden is not known, it is possible to compute the focusing functions $\mathbf{F}^+$ and $\mathbf{F}^-$ using an iterative scheme based on a variant of equation 8 and its time-reversed version. This forms the basis of the Marchenko imaging procedure Rose (2002); Wapenaar et al. (2013), that relies on the reflection response from the surface and a macro velocity model of the overburden as the only prior knowledge. In contrast, the work presented here relies on a much stronger assumption - i.e. the knowledge of the upper medium parameters - but allows in

turn a more direct way to compute $\mathbf{F}^+$ and $\mathbf{F}^-$ based on the inversion of $\mathbf{T}^{\mathbf{U}}$.

By injecting the focusing functions $\mathbf{F}^+$ in the full medium (Figure 1(a)), we obtain

$$\mathbf{R}\mathbf{F}^+ = \mathbf{F}^- + \mathbf{G}^+ \quad , \tag{9}$$

where $\mathbf{G}^+$ is the Green's function matrix in the full medium for downgoing sources at depth z_1. Equation 9 is graphically illustrated in Figure 3(b). The Green's functions $\mathbf{G}^+$ emerge as the focusing wavefields create virtual downgoing sources at depth z_1 in the full medium. By replacing the expressions of the focusing functions $\mathbf{F}^+$ and $\mathbf{F}^-$ (equations 7&8) into equation 9, we obtain

$$\mathbf{G}^+ = \left[\mathbf{R} - \mathbf{R}^{\mathbf{U}}\right]\left[\mathbf{T}^{\mathbf{U}}\right]^{-1} \quad . \tag{10}$$

The matrix $\mathbf{G}^-$, that contains the responses to upgoing sources at z_1, can be expressed using $\mathbf{G}^+$ as well as the matrices $\mathbf{R}_1^{\mathbf{U}}$ and $\mathbf{T}_1^{\mathbf{U}}$ obtained in the upper medium according to

$$\mathbf{G}^- = \mathbf{T}_1^{\mathbf{U}} + \mathbf{G}^+\mathbf{R}_1^{\mathbf{U}} \quad . \tag{11}$$

This relation is illustrated in Figure 3(c). Equation 11 is a decomposition of $\mathbf{G}^-$ into the portion of the wavefield that only travels in the upper medium $\mathbf{T}_1^{\mathbf{U}}$, and the portion of the wavefield that travels into the full medium $\mathbf{G}^+\mathbf{R}_1^{\mathbf{U}}$.

We finally replace these expressions of the Green's function matrices $\mathbf{G}^+$ and $\mathbf{G}^-$ into equation 6, to compute the objective virtual data set $\mathbf{R}_1^{\mathbf{L}}$ as

$$\begin{aligned}\mathbf{R}_1^{\mathbf{L}} &= \left[\mathbf{G}^-\right]^{-1}\mathbf{G}^+ \\ &= \left[\mathbf{T}_1^{\mathbf{U}} + \mathbf{G}^+\mathbf{R}_1^{\mathbf{U}}\right]^{-1}\left[\mathbf{R} - \mathbf{R}^{\mathbf{U}}\right]\left[\mathbf{T}^{\mathbf{U}}\right]^{-1} \\ &= \left[\mathbf{T}^{\mathbf{U}}\left[\mathbf{R} - \mathbf{R}^{\mathbf{U}}\right]^{-1}\mathbf{T}_1^{\mathbf{U}} + \mathbf{R}_1^{\mathbf{U}}\right]^{-1}\end{aligned} \tag{12}$$

As intended, this expression of the objective reflection matrix $\mathbf{R}_1^{\mathbf{L}}$ (or redatumed data set) is a function only of the initial surface data set $\mathbf{R}$ and of the matrices $\mathbf{R}^{\mathbf{U}}$, $\mathbf{R}_1^{\mathbf{U}}$, $\mathbf{T}^{\mathbf{U}}$ and $\mathbf{T}_1^{\mathbf{U}}$. Note that $\mathbf{R}^{\mathbf{U}}$, $\mathbf{R}_1^{\mathbf{U}}$, $\mathbf{T}^{\mathbf{U}}$ and $\mathbf{T}_1^{\mathbf{U}}$ depend only on the prior knowledge of the overburden.

3 NUMERICAL EXAMPLES

3.1 Seismic data set

To illustrate the method, we generate a synthetic seismic data set with 2D acoustic numerical simulations. We use the software developed by Thorbecke and Draganov (2011), based on a finite-difference scheme. The velocity model of the full medium is presented in Figure 6(a) and is 2000 m wide by 2000 m deep. It consists of three homogeneous layers separated by two non-horizontal boundaries, whose velocities are 1600 m/s, 2200 m/s and 2800 m/s, and whose densities are 1000 kg/m^3, 2000 kg/m^3 and 3000 kg/m^3.

The new datum is located below the first two layers at depth $z = 1000$ m. Two circular inclusions with vanishing velocity and of diameters 80 m and 160 m are placed in the homogeneous third layer, below the new datum, and represent targets to be detected. We have free-surface boundary conditions at the upper boundary and absorbing conditions at the other boundaries.

The initial reflection data set $\mathbf{R}$ is generated using $N = 126$ sources and receivers located a quarter wavelength below the free surface, corresponding to a sensor spacing of 16 m. The monopole (explosive) sources are modeled with a Ricker wavelet of central frequency 25 Hz. The spatial step of the grid is 4 m and the temporal step is 0.8 ms. An example of a common-source gather shows primary and multiple scattering events from both the overburden and the two targets (Figure 6(b)). The primary scattering events from the targets, partially screened by overburden multiples, arrive at 1.6 s and 1.9 s at $x = 0$ m.

The redatuming procedure starts with simulations in the upper medium, that corresponds to our prior knowledge of the overburden (Figure 4(a)). We place $N = 126$ sources and receivers at the free surface and another $N = 126$ sources and receivers at the new datum. This allows us to calculate the reflection and transmission matrices $\mathbf{R}^{\mathbf{U}}$, $\mathbf{R}_1^{\mathbf{U}}$, $\mathbf{T}^{\mathbf{U}}$ and $\mathbf{T}_1^{\mathbf{U}}$.

We compute the focusing functions $\mathbf{F}^+ = \left[\mathbf{T}^{\mathbf{U}}\right]^{-1}$ (see equation 7) using a Singular Value Decomposition (SVD) of $\mathbf{T}^{\mathbf{U}}$. We then construct the downgoing and upgoing Green's function matrices $\mathbf{G}^+$ and $\mathbf{G}^-$ following equations 10 and 11. Finally, we compute the objective redatumed data set $\mathbf{R}_1^{\mathbf{L}}$ following equation 12. The inverse of $\mathbf{G}^-$ is obtained using another SVD.

An example of a common-source gather from the redatumed data set is shown in Figure 5(a). The two dominant events correspond to primary scattering on the two targets and the two following events correspond to target multiples. As intended, the redatumed data set corresponds to a virtual acquisition made at depth $z = 1000$ m, and for which the imprint of the overburden is completely removed.

For comparison, a synthetic version of the objective data set is shown in Figure 5(b). This synthetic data set is obtained from a numerical simulation performed in the objective medium shown in Figure 4(b). We also present a comparison of three individual traces from the redatumed and synthetic data sets corresponding to three different receiver offsets (Figure 7).

The two primaries and first two multiples are observed in both the redatumed and the synthetic data set. The difference in shape and amplitude of the events at large offset is caused by the limited aperture of the surface array. Some weak acausal events are present in the redatumed data set. These events are again related to the finite aperture of the surface array, and are caused by the diffraction of the focusing function emitted at the edges of the array. This effect could possibly be atten-

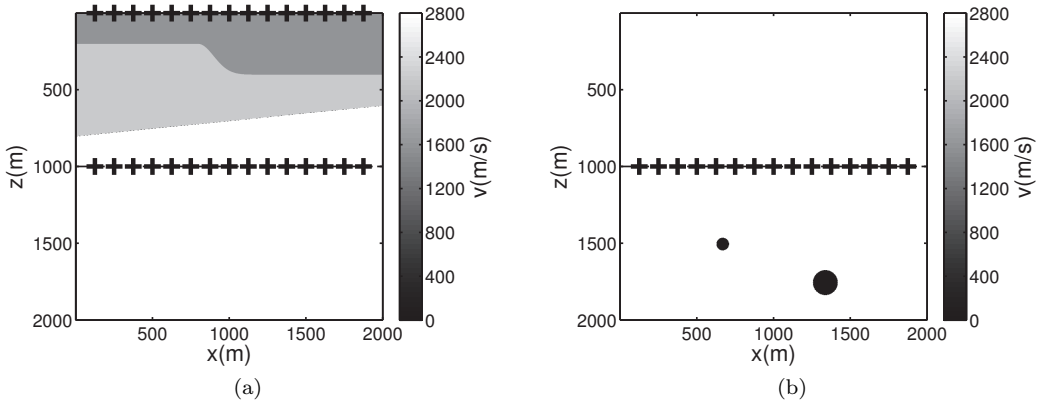

Figure 4. (a) Upper medium with free surface, overburden and homogeneous conditions below the new datum $z = 1000$ m. (b) Objective medium with two targets below the new datum $z = 1000$ m and homogeneous conditions above. A subpart of the (virtual) sources and receivers are denoted by the black crosses.

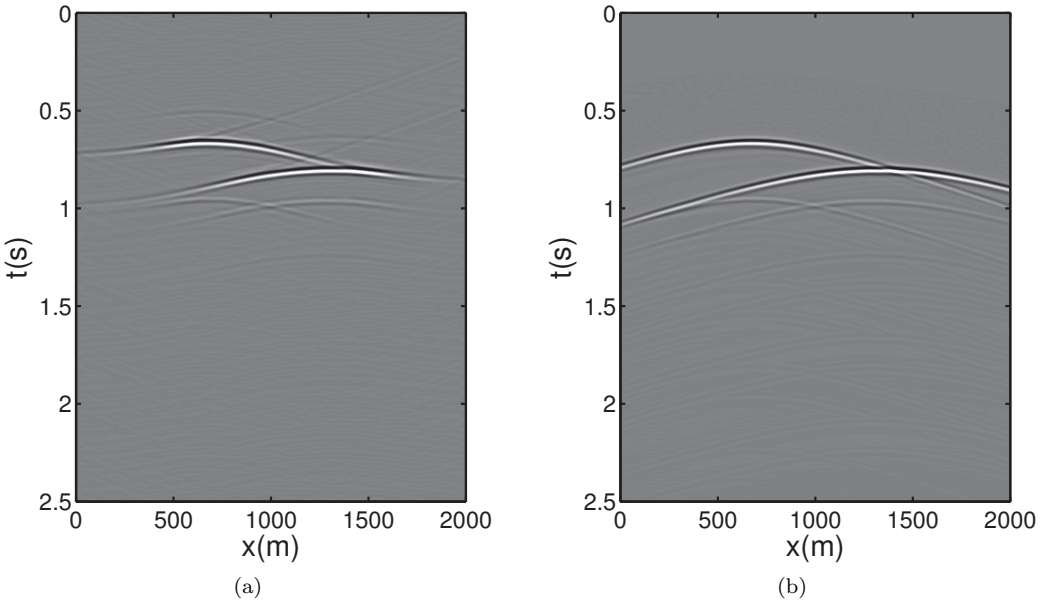

Figure 5. Common-source gather from: (a) the redatumed seismic data set $\mathbf{R_1^L}$ and (b) a synthetic numerical simulation in the objective medium. The (virtual) source is located at position $x = 992$ m along the new datum.

uated by using spatial tapering techniques during the inversion of the focusing function. The attenuation of these artifacts, also expected to occur in standard redatuming techniques, is beyond the scope of this study.

3.2 Acoustic data set

We generate another synthetic data set with 2D acoustic numerical simulations. This time, we use free-surface side boundaries to simulate a typical configuration encountered in acoustic nondestructive testing of materials. We use a custom made acoustic finite-difference scheme with constant density. We use the same velocity model, downsized to 1 m wide by 1 m deep (Figure 8(a)). The new datum is now located at depth $z = 50$ cm and the two circular targets are of diameter 4 cm and 8 cm.

The initial reflection data set $\mathbf{R}$ is generated using $N = 125$ sources and receivers located one grid-point (0.5 mm) below the free surface, corresponding to a sensor spacing of 0.8 cm. The monopole (explosive) sources are modeled with a Ricker wavelet of central frequency 50 kHz. The spatial step of the grid is 0.5 mm and the temporal step is 0.11 μs. An example of a common-source gather shows primary and multiple scattering events from the overburden, the two targets and the side boundaries (Figure 8(b)). The primary scattering

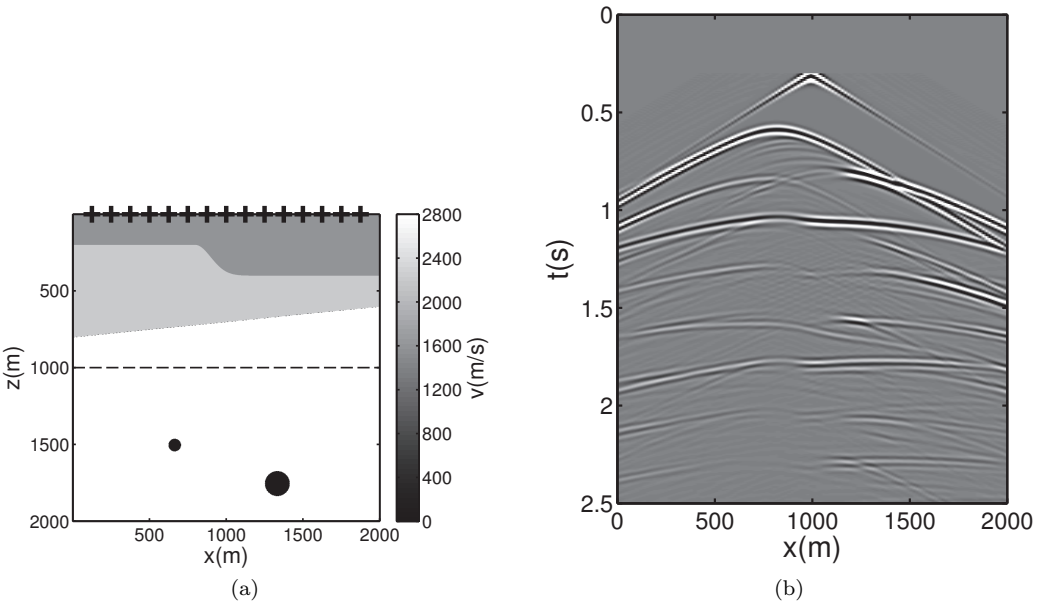

Figure 6. (a) Full seismic medium including the free surface, the overburden, and the two targets. A subpart of the sources and receivers are denoted by the black crosses. (b) Common-source gather for a source at $x = 992$ m.

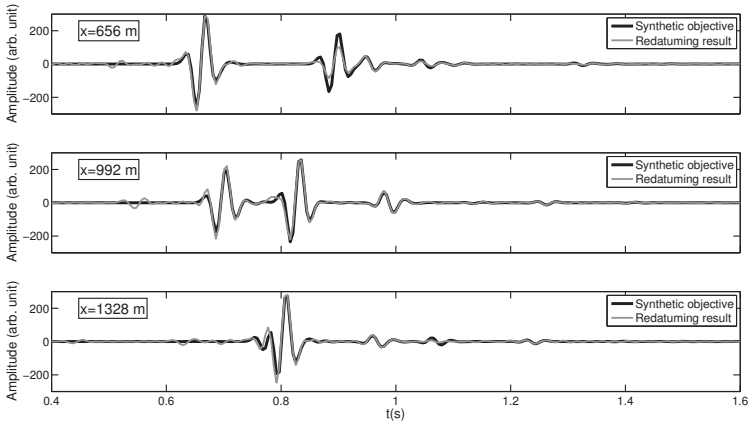

Figure 7. Comparison of redatumed and synthetic seismic traces at three different receiver offsets, $x = 656$ m, $x = 992$ m and $x = 1328$ m. The (virtual) source is located at position $x = 992$ m along the new datum.

events from the targets, partially screened by overburden multiples and side reflections, arrive at 1 ms and 1.2 ms at $x = 0$ cm.

We follow the procedure detailed in the previous section to compute the objective redatumed data set $\mathbf{R}_1^{\mathbf{L}}$. An example of a common-source gather from the redatumed data set is shown in Figure 9(a). The two dominant events correspond to primary scattering on the two targets and the following events correspond to target and side-boundary multiples. As intended, the redatumed data set corresponds to a virtual acquisition made at depth $z = 50$ cm, and for which the imprint of the overburden is completely removed. For comparison, a synthetic version of the objective data set is shown in Figure 9(b). We also present a comparison of three individual traces from the redatumed and synthetic data sets corresponding to three different receiver offsets (Figure 10).

A good agreement is observed between the redatumed and the synthetic data set. In contrast with the absorbing-side-boundaries case, the differences in shape and amplitude of the events at large offset are much less pronounced. The acausal events due to diffraction of the focusing function at the edges of the surface array are also less noticeable. The presence of the reflective boundaries increase the effective aperture of the surface

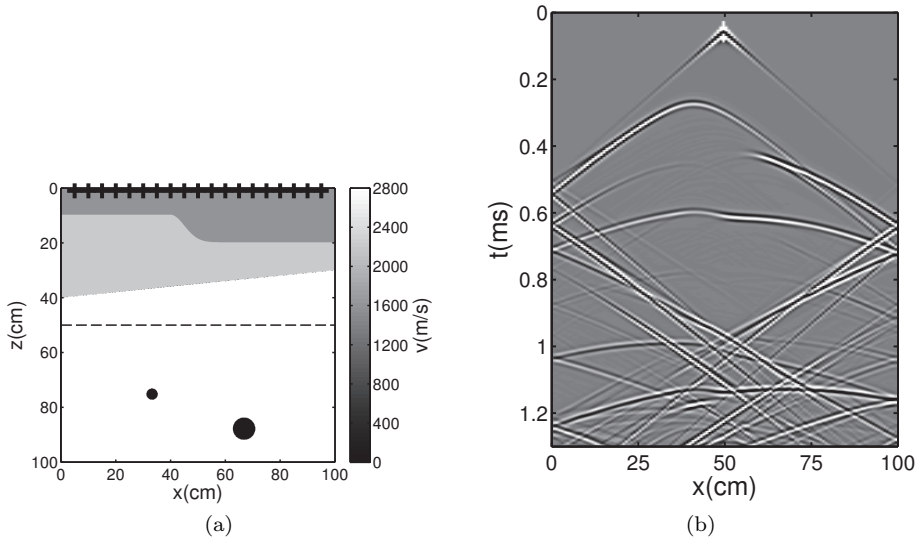

Figure 8. (a) Full acoustic medium including the free surface at the top and side boundaries, the overburden, and the two targets. A subpart of the sources and receivers are denoted by the black crosses. (b) Common-source gather with source at position $x = 50$ cm.

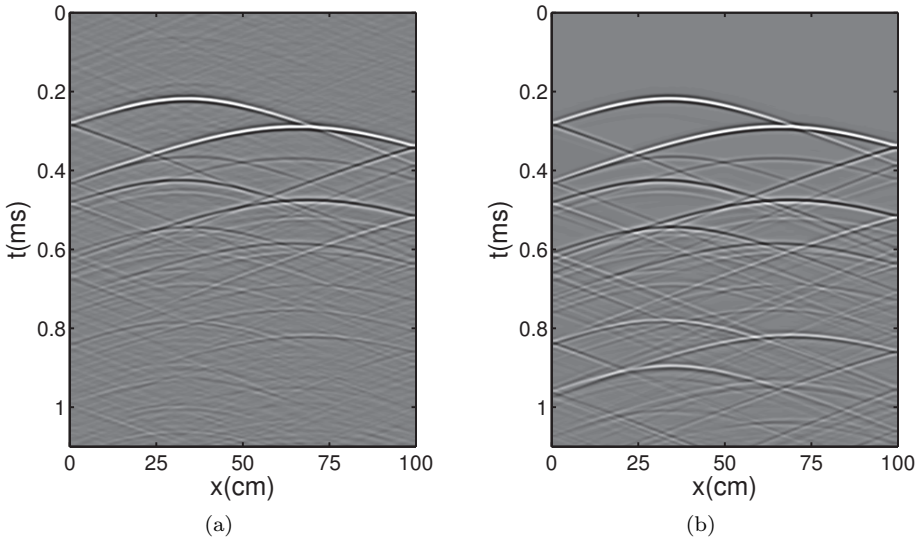

Figure 9. Common-source gather from: (a) the redatumed acoustic data set $\mathbf{R_1^L}$ and (b) a synthetic numerical simulation in the objective medium. The (virtual) source is located at position $x = 50$ cm along the new datum.

array and thus improves the reconstruction of the redatumed data set.

4 CONCLUSION

We introduced a model-based redatuming technique that correctly handles surface multiples and internal multiples in the overburden. The technique relies on the assumption that a detailed knowledge of the model parameters is available above the new datum.

In addition to a formal derivation of the redatuming equations, we presented an intuitive graphics-based derivation supported by a matrix formalism. The redatuming procedure can be summarized as follows:

(i) Use numerical simulations to compute reflection and transmission matrices of the overburden.

(ii) Through an inversion step, retrieve the focusing functions that give rise to downgoing virtual sources at the new datum.

(iii) Using the initial data set and the simulated

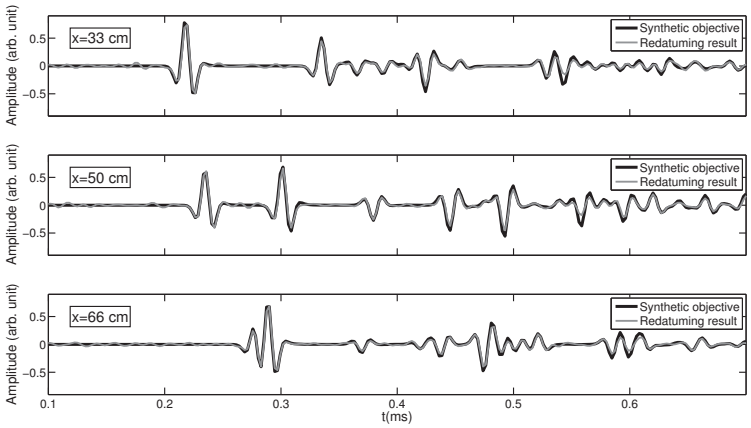

Figure 10. Comparison of redatumed and synthetic acoustic traces at three different receiver offsets, $x = 33$ cm, $x = 50$ cm and $x = 66$ cm. The (virtual) source is located at position $x = 50$ cm along the new datum.

overburden matrices, compute the surface responses to downgoing and upgoing virtual sources at the new datum.

(iv) Use the reponses to these virtual sources to evaluate the redatumed data set through multi-dimensional deconvolution.

The redatumed data set corresponds to a virtual reflection response acquired at the new datum, and for which the imprint of the overburden is completely removed.

We demonstrated the procedure on two synthetic data sets generated in 2D acoustic media. The first medium had absorbing side boundaries to simulate a seismic data set while the other medium had free-surface side boundaries to simulate an acoustic nondestructive testing data set. In both cases, the redatuming procedure successfully allowed to retrieve primary and multiple scattering events from targets located below the overburden. The absence of surface multiples and internal multiple showed that the imprint of the overburden was fully removed. The redatumed seismic data set suffered from finite-aperture effects of the surface array, as it can be expected from any other standard redatuming procedure. The redatumed acoustic data set did not suffer these limitations as the side boundaries artificially increased the effective aperture of the surface array.

This technique requires a stronger prior knowledge than the Marchenko imaging procedure to compute the focusing functions. However, it can provide a simpler and more direct way to perform the redatuming in cases where a good knowledge of the overburden is available. Indeed, the interest of the technique lies in the fact that the inversion of the transmission matrix automatically generates a focus free of multiples and compensates for effects such as attenuation, irregular topography and irregular spatial sampling.

The extrapolation of the method to 3D acoustic data should be straightforward; however, the application to elastic data should be carefully tested. Based on recent progresses in elastic Marchenko imaging da Costa Filho et al. (2014); Wapenaar (2014), we believe that elastic redatuming could also be achieved. The limitation in the elastic case would probably come from the ability to have a detailed knowledge of much more model parameters.

ACKNOWLEGDMENTS

We thank the sponsors of the Consortium Project on Seismic Inverse Methods for Complex Structures.

REFERENCES

Aubry, J.-F., M. Tanter, J. Gerber, J.-L. Thomas, and M. Fink, 2001, Optimal focusing by spatio-temporal inverse filter. ii. experiments. application to focusing through absorbing and reverberating media: The Journal of the Acoustical Society of America, **110**, 48–58.

Berryhill, J. R., 1979, Wave-equation datuming: Geophysics, **44**, 1329–1344.

Broggini, F., R. Snieder, and K. Wapenaar, 2014, Data-driven wavefield focusing and imaging with multidimensional deconvolution: Numerical examples from reflection data with internal multiples: Geophysics, **79**, WA107–WA115.

da Costa Filho, C. A., M. Ravasi, A. Curtis, and G. A. Meles, 2014, Elastodynamic green's function retrieval through single-sided marchenko inverse scattering: Phys. Rev. E, **90**, no. 6, 063201.

Mulder, W. A., 2005, Rigorous redatuming: Geophysical Journal International, **161**, 401–415.

Rose, J. H., 2002, Single-sided autofocusing of sound in layered materials: Inverse Problems, **18**, 1923.

Schuster, G. T., and M. Zhou, 2006, A theoretical

overview of model-based and correlation-based redatuming methods: Geophysics, **71**, SI103–SI110.
Shtivelman, V., and A. Canning, 1988, Datum correction by wave-equation extrapolation: Geophysics, **53**, 1311–1322.
Tanter, M., J.-F. Aubry, J. Gerber, J.-L. Thomas, and M. Fink, 2001, Optimal focusing by spatio-temporal inverse filter. i. basic principles: The Journal of the Acoustical Society of America, **110**, 37–47.
Thorbecke, J. W., and D. Draganov, 2011, Finite-difference modeling experiments for seismic interferometry: Geophysics, **76**, H1–H18.
Wapenaar, C., and A. Berkhout, 1989, Elastic wave field extrapolation: Redatuming of single- and multi-component seismic data: Elsevier. Advances in exploration geophysics.
Wapenaar, K., 2014, Single-sided marchenko focusing of compressional and shear waves: Phys. Rev. E, **90**, no. 6, 063202.
Wapenaar, K., F. Broggini, E. Slob, and R. Snieder, 2013, Three-dimensional single-sided marchenko inverse scattering, data-driven focusing, greens function retrieval, and their mutual relations: Physical Review Letters, **110**, 084301.
Wapenaar, K., E. Slob, and R. Snieder, 2008, Seismic and electromagnetic controlled-source interferometry in dissipative media: Geophys. Prosp., **56**, 419–434.
Wapenaar, K., J. Thorbecke, J. van der Neut, F. Broggini, E. Slob, and R. Snieder, 2014, Green's function retrieval from reflection data, in absence of a receiver at the virtual source position: The Journal of the Acoustical Society of America, **135**, 2847–2861.
Wapenaar, K., and J. van der Neut, 2010, A representation for greens function retrieval by multidimensional deconvolution: The Journal of the Acoustical Society of America, **128**, EL366–EL371.

A RECIPROCITY THEOREMS

Consider two independent wave states A and B, defined by medium parameters (ρ_A, κ_A) and (ρ_B, κ_B) and source terms f_A and f_B. If inside a volume V enclosed by a surface S, the medium parameters are the same for state A and state B, a special case of Rayleigh's reciprocity theorem Wapenaar and Berkhout (1989) gives

$$\oint_S \frac{1}{\rho}\left[p_A \boldsymbol{\nabla} p_B - p_B \boldsymbol{\nabla} p_A\right].\mathrm{d}\boldsymbol{S} = \int_V \frac{1}{\rho}\left[p_A f_B - p_B f_A\right]\mathrm{d}V \quad . \tag{13}$$

This relation is valid for arbitrary and independent source terms f_A and f_B. The medium parameters outside the integration volume V can also be different for states A and B. By choosing $f_B = \rho(\boldsymbol{r})\delta(\boldsymbol{r} - \boldsymbol{r_0})$ and $f_A = 0$, we obtain the special case known as the representation theorem

$$p(\boldsymbol{r_0}) = \oint_S \frac{1}{\rho}\left[p(\boldsymbol{r})\boldsymbol{\nabla} g(\boldsymbol{r}, \boldsymbol{r_0}) - g(\boldsymbol{r}, \boldsymbol{r_0})\boldsymbol{\nabla} p(\boldsymbol{r})\right]\cdot \mathrm{d}\boldsymbol{S} \quad . \tag{14}$$

A.1 Case with a free surface

Consider a volume V enclosed by a surface S composed of a free surface and a virtual horizontal boundary S_1 at an arbitrary depth, as represented in Figure 11(a). The coordinate x^1 denotes the horizontal position along the boundary S_1 and z is the depth coordinate. Because the pressure vanishes at the free surface, and because the boundary S_1 is orthogonal to the z axis, the reciprocity theorem (equation 13) simplifies to

$$\begin{aligned}&\int_{S_1} \frac{1}{\rho(x^1)}\left[p_A(x^1)\partial_z p_B(x^1) - p_B(x^1)\partial_z p_A(x^1)\right]\mathrm{d}x^1 \\ &\qquad = \int_V \frac{1}{\rho}\left[p_A f_B - p_B f_A\right]\mathrm{d}V \quad .\end{aligned} \tag{15}$$

This also supposes that the depth of S_1 is much smaller than the medium width, so that the side contributions to the surface integral can be neglected. By decomposing p_A and p_B as upgoing and downgoing wavefields at S_1, the left-hand side of equation 15 can be expanded into the four following terms:

$$\begin{aligned}&\int_{S_1} \frac{1}{\rho(x^1)}\left[p_A^+\partial_z p_B^- + p_A^-\partial_z p_B^+\right]\mathrm{d}x^1 \\ &- \int_{S_1} \frac{1}{\rho(x^1)}\left[p_B^+\partial_z p_A^- + p_B^-\partial_z p_A^+\right]\mathrm{d}x^1 \\ &+ \int_{S_1} \frac{1}{\rho(x^1)}\left[p_A^+\partial_z p_B^+ + p_A^-\partial_z p_B^-\right]\mathrm{d}x^1 \\ &- \int_{S_1} \frac{1}{\rho(x^1)}\left[p_B^+\partial_z p_A^+ + p_B^-\partial_z p_A^-\right]\mathrm{d}x^1 \quad .\end{aligned} \tag{16}$$

Assuming that there are no reflector crossing the boundary S_1, i.e., $\partial_z\rho(x^1)$=0 and $\partial_z\kappa(x^1)$=0, the upgoing and downgoing wavefields are locally decoupled. Using the one-way wave equation at S_1, it can be shown that the first and second terms of expression 16 are equal to each other, and that the third and fourth terms cancel each other out Wapenaar and Berkhout (1989). The reciprocity theorem can thus be written as

$$\begin{aligned}&\int_{S_1} \tfrac{2}{\rho(x^1)}\left[p_A^+(x^1)\partial_z p_B^-(x^1) + p_A^-(x^1)\partial_z p_B^+(x^1)\right]\mathrm{d}x^1 \\ &\qquad = \int_V \frac{1}{\rho}\left[p_A f_B - p_B f_A\right]\mathrm{d}V \quad .\end{aligned} \tag{17}$$

This special form of the reciprocity theorem is used in the next section to derive equations 10 and 11 of the redatuming technique. We also use equation 17 to derive an identity that is used in the following. For wave state A, let us consider the case of an impulsive source

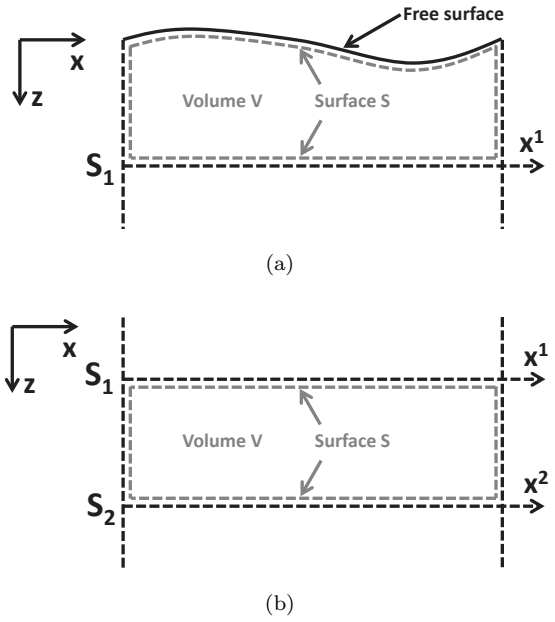

Figure 11. Schematic representation of the integration volumes for the derivation of the reciprocity theorems with a free surface (a), and without a free surface (b).

$f_A = \rho\delta(x^1 - x_i^1)$ at a distance $\epsilon \to 0$ above x_i^1. For wave state B, an impulsive source $f_B = \rho\delta(x^1 - x_j^1)$ is located at a distance $\epsilon \to 0$ below x_j^1. Assuming that the medium is homogeneous outside the volume V, equation 17 simplifies to

$$\int_{S_1} \frac{2}{\rho(x^1)} p_A(x^1)\partial_z p_B^-(x^1)\mathrm{d}x^1 = -p_B(x_i^1) \quad , \qquad (18)$$

where we note that $p_A^-(x^1) = 0$ and thus $p_A(x^1) = p_A^+(x^1)$. We also used the fact that $f_B = 0$ in the integration volume V. As epsilon goes to zero, the wave states A and B become symmetrically equivalent and we have $p_A(x_j^1) = p_B(x_i^1)$. We then deduce from equation 18 the identity

$$\partial_z p_B^-(x^1) = -\frac{\rho(x^1)}{2}\delta(x^1 - x_j^1) \quad . \qquad (19)$$

This expression describes the vertical derivative of the upgoing pressure field just above an impulsive source.

A.2 Case without a free surface

Consider now a volume V enclosed by a surface S composed of two virtual horizontal boundaries S_1 and S_2, as represented in Figure 11(b). The coordinate x^1 (resp. x^2) denotes the horizontal position along the boundary S_1 (resp. S_2) and z is the depth coordinate. Because the surface S enclosing the volume V does not include a free surface, the surface integral needs to be expressed at S_1 and S_2. We further assume that there are no sources in the volume V, so that the reciprocity theorem (equation 13) simplifies to

$$\int_{S_1} \frac{1}{\rho(x^1)} \left[p_A(x^1)\partial_z p_B(x^1) - p_B(x^1)\partial_z p_A(x^1)\right] \mathrm{d}x^1$$

$$= \int_{S_2} \frac{1}{\rho(x^2)} \left[p_A(x^2)\partial_z p_B(x^2) - p_B(x^2)\partial_z p_A(x^2)\right] \mathrm{d}x^2 \; . \qquad (20)$$

Similarly to the previous case, we use the upgoing and downgoing wavefield decomposition at boundaries S_1 and S_2. Assuming that there are no reflectors crossing S_1 and S_2, we obtain the one-way reciprocity theorem of the convolution type Wapenaar et al. (2014):

$$\int_{S_1} \frac{1}{\rho(x^1)} \left[p_A^+(x^1)\partial_z p_B^-(x^1) + p_A^-(x^1)\partial_z p_B^+(x^1)\right] \mathrm{d}x^1$$

$$= \int_{S_2} \frac{1}{\rho(x^2)} \left[p_A^+(x^2)\partial_z p_B^-(x^2) + p_A^-(x^2)\partial_z p_B^+(x^2)\right] \mathrm{d}x^2 \; ; . \qquad (21)$$

This relation is used in the next section to derive equation 6 of the redatuming technique.

B DERIVATION OF THE REDATUMING EQUATIONS

B.1 Definition of the different wave states

We define four different wave states that are used with the reciprocity theorems to derive the redatuming equations (Figure 12). The full medium is represented in

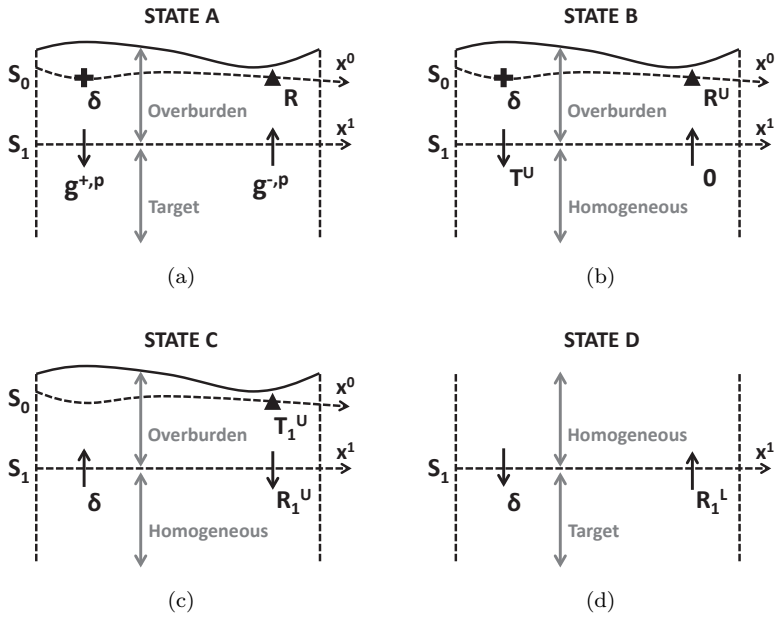

Figure 12. Illustration of wave states A, B, C and D used in the reciprocity theorems for the derivation of the redatuming equations.

state A, with an irregular free surface. The original reflection data acquisition is made along the boundary S_0 at an arbitrary depth below the free surface. The boundary S_0 can be curvilinear, and the acquisition spatial interval can be irregular. The positions of sources and receivers along the boundary S_0 are denoted by the coordinate x^0. The new datum boundary S_1 is located below the overburden and is set to be horizontal. The positions along the new datum are denoted by the coordinate x^1 and the spatial interval Δx is chosen to be constant. The target area lies below the new datum S_1.

For an impulse pressure source located at position x_i^0, the reflection response $R(x^0, x_i^0)$ is the pressure recorded along x^0. We also define the downgoing (resp. upgoing) wavefield at x^1 $g^{+,p}(x^1, x_i^0)$ (resp. $g^{-,p}(x^1, x_i^0)$). By reciprocity (equation 5), these are equal to the pressure response at x_i^0 for an upgoing (resp. downgoing) impulse source at x^1 $g^{p,-}(x_i^0, x^1)$ (resp. $g^{p,+}(x_i^0, x^1)$). These last two functions are the ones that we aim to determine to achieve the redatuming. In summary, we have

$$\begin{aligned} f_A &= \rho\delta(x^0 - x_i^0) \quad , \\ p_A(x^0) &= g(x^0, x_i^0) = R(x^0, x_i^0) \quad , \\ p_A^+(x^1) &= g^{+,p}(x^1, x_i^0) = g^{p,-}(x_i^0, x^1) \quad , \\ p_A^-(x^1) &= g^{-,p}(x^1, x_i^0) = g^{p,+}(x_i^0, x^1) \quad . \end{aligned} \tag{22}$$

Wave states B and C take place in the upper medium, that represents the overburden and that extends from the free surface to the new datum S_1. The medium below the new datum is homogeneous. We run two different simulation sets in this upper medium. For wave state B, an impulse pressure source is placed at x_j^0 and the reflection response $R^U(x^0, x_j^0)$ from S_0 to S_0 is recorded along x^0. The transmission response $T^U(x^1, x_j^0)$ from S_0 to S_1 is also recorded. We have

$$\begin{aligned} f_B &= \rho\delta(x^0 - x_j^0) \quad , \\ p_B(x^0) &= g^U(x^0, x_j^0) = R^U(x^0, x_j^0) \quad , \\ \partial_z p_B^+(x^1) &= \partial_z g^{U|+,p}(x^1, x_j^0) = \partial_z T^U(x^1, x_j^0) \quad , \\ \partial_z p_B^-(x^1) &= \partial_z g^{U|-,p}(x^1, x_j^0) = 0 \quad . \end{aligned} \tag{23}$$

where the superscript U denotes quantities computed in the upper medium. For wave state C, an impulse pressure source is placed at x_k^1 and the reflection response from S_1 to S_1 in the upper medium $R_1^U(x^1, x_k^1)$ is recorded along x^1. The transmission response $T_1^U(x^0, x_k^1)$ from S_1 to S_0 is also recorded. We have

$$\begin{aligned} f_C &= \rho\delta(x^1 - x_k^1) \quad , \\ p_C(x^0) &= g^U(x^0, x_k^1) = T_1^U(x^0, x_k^1) \quad , \\ \partial_z p_C^+(x^1) &= \partial_z g^U(x^1, x_k^1) = \partial_z R_1^U(x^1, x_k^1) \quad , \\ \partial_z p_C^-(x^1) &= -\rho\delta(x^1 - x_k^1)/2 \quad . \end{aligned} \tag{24}$$

where the source is located at a distance $\epsilon \to 0$ below S_1. The expression of $\partial_z p_C^-$ was derived in the previous section (equation 19). We note that in order to only retain downgoing energy in p_C^+, we remove the direct wave that propagates quasi-horizontally from $R_1^U(x^1, x_k^1)$.

Wave state D takes place in the objective medium, that represents the target area below the new datum S_1.

The medium above the new datum is homogeneous. The redatumed or objective data set corresponds to an acquisition made along S_1. For an impulse pressure source at x_l^1, the pressure wavefield measured at x^1 forms the reflection response $R_1^L(x^1, x_l^1)$. We have

$$\begin{aligned} f_D &= \rho\delta(x^1 - x_l^1) \quad , \\ \partial_z p_D^+(x^1) &= \rho\delta(x^1 - x_l^1)/2 \quad , \\ \partial_z p_D^-(x^1) &= \partial_z g^L(x^1, x_l^1) = \partial_z R_1^L(x^1, x_l^1) \quad . \end{aligned} \tag{25}$$

where the superscript L denotes quantities related to the objective (or lower) medium. The source is located at a distance $\epsilon \to 0$ above S_1. By antisymmetry with respect to the z-axis, we have $\partial_z p_D^+(x^1) = -\partial_z p_C^-(x^1)$. Because $p_D^-(x^1)$ only describe upgoing wavefields, we expect the direct wave to be absent from $R_1^L(x^1, x_l^1)$.

B.2 Derivation of the downgoing source Green's function matrix $\mathbf{G}^+$

This matrix represents the surface response at S_0 for a virtual downgoing source at the new datum S_1. We apply the reciprocity theorem (equation 17) to wave states A and B, to obtain

$$\begin{aligned} &\int_{S_1} \frac{2}{\rho(x^1)} g^{p,+}(x_i^0, x^1) \partial_z T^U(x^1, x_j^0) \mathrm{d}x^1 \\ &\qquad = R(x_i^0, x_j^0) - R^U(x_i^0, x_j^0) \quad , \end{aligned} \tag{26}$$

using the reciprocity relation $R(x_i^0, x_j^0) = R(x_j^0, x_i^0)$. A discretized version of this equation can be written as the matrix relation

$$\mathbf{G}^+ \mathbf{T}^{\mathbf{U}} = \mathbf{R} - \mathbf{R}^{\mathbf{U}} \quad , \tag{27}$$

where the matrices $\mathbf{R}$, $\mathbf{R}^{\mathbf{U}}$, $\mathbf{T}^{\mathbf{U}}$ and $\mathbf{G}^+$ are defined as

$$\begin{aligned} \{\mathbf{R}\}_{ij} &= R(x_i^0, x_j^0) \quad , \\ \{\mathbf{R}^{\mathbf{U}}\}_{ij} &= R^U(x_i^0, x_j^0) \quad , \\ \{\mathbf{T}^{\mathbf{U}}\}_{ij} &= \partial_z T^U(x_i^1, x_j^0) \quad , \\ \{\mathbf{G}^+\}_{ij} &= 2\Delta x g^{p,+}(x_i^0, x_j^1)/\rho(x_j^1) \quad . \end{aligned} \tag{28}$$

B.3 Derivation of the upgoing source Green's function matrix $\mathbf{G}^-$

This matrix represents the surface response at S_0 for a virtual upgoing source at the new datum S_1. We apply the reciprocity theorem (equation 17) to wave states A and C, to obtain

$$\begin{aligned} &-g^{p,-}(x_i^0, x_k^1) + \int_{S_1} \frac{2}{\rho(x^1)} g^{p,+}(x_i^0, x^1) \partial_z R_1^U(x^1, x_k^1) \mathrm{d}x^1 \\ &\qquad = -T_1^U(x_i^0, x_k^1) \quad , \end{aligned} \tag{29}$$

using the fact that $f_C = 0$ in the integration volume V. A discretized version of this equation can be written as the matrix relation

$$\mathbf{G}^- = \mathbf{T}_1^{\mathbf{U}} + \mathbf{G}^+ \mathbf{R}_1^{\mathbf{U}} \quad , \tag{30}$$

where the matrices $\mathbf{R}_1^{\mathbf{U}}$, $\mathbf{T}_1^{\mathbf{U}}$ and $\mathbf{G}^-$ are defined as

$$\begin{aligned} \{\mathbf{R}_1^{\mathbf{U}}\}_{ij} &= \partial_z R_1^U(x_i^1, x_j^1) \quad , \\ \{\mathbf{T}_1^{\mathbf{U}}\}_{ij} &= T_1^U(x_i^0, x_j^1) \quad , \\ \{\mathbf{G}^-\}_{ij} &= g^{p,-}(x_i^0, x_j^1) \quad . \end{aligned} \tag{31}$$

B.4 Derivation of the redatumed reflection response $\mathbf{R_1^L}$

This matrix contains the redatumed data set that simulates an acquisition made at S_1 and for which the imprint of the overburden is completely removed. We apply the one-way reciprocity theorem (equation 21) to wave states A and D, and choose a virtual boundary S_2 to be below the deepest reflector of the target area. Because there is no upgoing energy at this boundary, the one-way reciprocity theorem (equation 21) simplifies to

$$\int_{S_1} \frac{1}{\rho(x^1)} \left[p_A^+(x^1) \partial_z p_D^-(x^1) + p_A^-(x^1) \partial_z p_D^+(x^1) \right] \mathrm{d}x^1 = 0 \, . \tag{32}$$

We replace the expressions of $\partial_z p_D^+$, $\partial_z p_D^-$, p_A^+ and p_A^-, to obtain

$$\int_{S_1} \frac{1}{\rho(x_1)} g^{p,-}(x_i^0, x^1) \partial_z R_1^L(x^1, x_l^1) \mathrm{d}x_1 = -\frac{1}{2} g^{p,+}(x_i^0, x_l^1) \, . \tag{33}$$

A discretized version of this equation can be written as the matrix relation

$$\mathbf{G}^+ = \mathbf{G}^- \mathbf{R}_1^{\mathbf{L}} \quad , \tag{34}$$

where the matrix $\mathbf{R}_1^{\mathbf{L}}$ is defined as

$$\{\mathbf{R}_1^{\mathbf{L}}\}_{ij} = -4(\Delta x)^2 \frac{\partial_z R_1^L(x_i^1, x_j^1)}{\rho(x_i^1)\rho(x_j^1)} \quad . \tag{35}$$